Is amino-modification of HKUST-1 in PEI mixed-matrix membranes always favorable to CO 2 separation?

Ge Yang, Yanjiao Wang, Mengling Sun, Panpan Xu, Chunzheng Wang, Ke Huang, Heqing Jiang, Svetlana Mintova, Hailing Guo

Is amino-modification of HKUST-1 in PEI mixed-matrix membranes always favorable to CO_2 separation?

Ge Yang[a,b], Yanjiao Wang[a], Mengling Sun[a], Panpan Xu[a], Chunzheng Wang[a], Ke Huang[a], Heqing Jiang[c], Svetlana Mintova[a,d], Hailing Guo[a,*]

a State Key Laboratory of Heavy Oil Processing, College of Chemistry and Chemical Engineering, China University of Petroleum (East China) Qingdao, 266555 (P.R. China).
b College of Science, China University of Petroleum (East China), Qingdao, 266555 (P.R. China).
c Qingdao Institute of Bioenergy and Bioprocess Technology, Chinese Academy of Sciences, Laoshan District, Qingdao CN-266101, China
d Laboratoire Catalyse et Spectrochimie (LCS), ENSICAEN, UNICAEN, CNRS, Normandie Université, 6 boulevard du Marechal Juin, 14050 Caen (France).

* Corresponding Author Email: guohl@upc.edu.cn

1 Introduction

Gas separation processes play important roles in industry production and daily life. Compared with chemical separation processes with high energy consumption, membrane based separation technology shows the advantages of high energy efficiency and easy operation[1, 2]. Polymeric membranes are attractive for membrane separation since they are economical and easily fabricated. While, due to the trade-off effect between permeability and selectivity in polymeric membranes, mixed matrix membranes (MMMs) loaded with various fillers including porous materials have received considerable attention since they combine the properties of the filler and the matrix, showing the potential to break performance limits[3,5]. Among the various fillers used, the MOFs are widely considered because the organic linkers enable potentially stronger interaction with the polymers.

However, the separation performance of most MMMs is under the performance upper boundary due to the effects of multiple factors such as loading, dispersion in casting solvent, and interface compatibility[6]. These factors determine the efficiency of the filler phase and the state of non-selective interfacial voids in MMMs. Although MOFs materials have shown stronger and better regulated "polymer-filler" interactions, compared with other porous materials, the structural optimization of MOFs-based MMMs is still the critical factor to develop high-performance MMMs[7,9]. The main effective structural optimization strategies include reduction of filler's particle size, synthesis of nanosheets, modification of filler's surface or polymer chains by functional groups, *in-situ* membrane preparation[6, 9,11]. In general, grafting functional groups onto MOFs has been considered as one of the best techniques since is easily achieved by substituting the MOFs' functional ligand. Vankelecom's research on UiO-66-based MMMs found that NH_2-UiO-66 could not only enhanced the interactions between the filler and the matrix, but also improve the adsorption of CO_2 in NH_2-UiO-66, which was conducive to the separation of CO_2/CH_4[12]. Similar performance optimizations have been reported for NH_2-UiO-66/PMMA MMMs[13],

NH_2-MIL-53/Pebax MMMs[14], NH_2-MIL-53/PI MMMs[15], NUS-8/PIM-1[16]. The main focus is on the design of high-performing MOF-based MMMs with molecule sieving features and reinforced interface.

According to previous reports, the MMMs are not effective in H_2/CO_2 separation[6, 17]. Due to the close molecular kinetic diameters of H_2 and CO_2 molecules and the stronger polarity of CO_2, neither sieving effect nor adsorption enhancement effect can significantly improve the performance of MMMs, especially the H_2/CO_2 selectivity. In our recent work, we combined HKUST-1 nanoparticles with Polyetherimide(PEI) and the resulted MMMs were used for H_2/CO_2 separation[18]. The PEI is a high-performance polymer with superior processability, which could be molded into different forms[19]. HKUST-1 ($Cu_3(BTC)_2$) is a porous materials with channels size of 9 Å, allowing the rapid permeation of gas molecules, but with low molecule sieving property [17]. The HKUST-1 has not been widely used for preparation of MMMs like the UiO series, MIL series and ZIFs crystals[6]. Our work took advantage of the large pore of HKUST-1 nanocrystals to accelerate H_2 diffusion with low diffusion resistance. Whereas, the permeability of CO_2 molecules was affected by adsorption-desorption process in the HKUST-1, resulting in a higher diffusion resistance. The phenomenon of increased H_2 permeability accompanied by decreased CO_2 permeability was also observed by Liu [20]. The separation mechanism of HKUST-1/PEI MMMs controlled by "adsorption-diffusion" of H_2/CO_2 was proposed. Based on this mechanism, we postulated that by increasing the adsorption-desorption resistance of HKUST-1 to CO_2, permeance could improve the MMMs' performance by amino-functionalization of the HKUST-1. The *in-situ* functionalization of HKUST-1 is difficult, as its ligands (Trimesic acid, BTC) cannot be completely replaced by functional ligands. NH_2-functionalized HKUST-1 has been prepared by partial replacement of the BTC with NH_2-BDC[21,23]. Sun reported on the synthesis of sub-NH_2-Cu-BTC with 2 μm crystal size resulting in stronger affinity between NH_2-Cu-BTC and CO_2 molecules[21]. Concerning the NH_2-HKUST-1 crystals, the final substitution ratio and position of amino-functionalized ligands have not been studied before, thereby the actual effect from the incomplete amino-functionalization is not clear.

Herein, we report the amino- functionalization of HKUST-1 crystals for enhancement of the diffusion resistance of CO_2 in MMMs. The modification procedure and the position of the amino groups on HKUST-1 crystals were studied in details.

2 Experimental section

2.1 Materials

Copper (II) nitrate trihydrate ($Cu(NO_3)_2 \cdot 3H_2O$, 99.0%–102%) and sodium formate (HCOONa, ≥99%) were bought from Sinopharm Chemical Reagent Co., Ltd. (China). 1,3,5-benzenetricarboxylic acid, 2-aminoterephthalic acid, ethanol (C_2H_5OH) and dichloromethane (CH_2Cl_2) were obtained from Shanghai Aladdin Biochemical Technology Co., Ltd. (China). Polyetherimide (PEI) particles was supplied by

SABIC. The deionized water was homemade.

2.2 Synthesis of HKUST-1 and NH_2-HKUST-1 materials

The HKUST-1 nanocrystals were synthesized following the methodology reported earlier[18]. Solution A was obtained by dissolving Cu $(NO_3)_2 \cdot 3H_2O$ (1.09 g) in deionized water (36.0 ml), and solution B was prepared by mixing 1,3,5-benzenetricarboxylic acid (0.63 g) with sodium formate (0.94g) in ethanol (36.0 mL).Then, solution B was slowly added in drops to solution A with magnetic stirring (600 rpm), and then the mixture was transferred to a teflon autoclave for crystallization at 120 °C for 3 h. The as-synthesized product was purified using a centrifuge (5000 rpm, 15 min) and re-dispersed in deionized water; the procedure was repeated three times and finally stabilized in ethanol. The product was freeze-dried and the sample was denoted as HKUST-1. The *in-situ* ammonia functionalized sample named NH_2-HKUST-1 was prepared only changing the solution B including dissolution of 0.47g 1,3,5-Benzenetricarboxylic acid, 0.14g 2-Aminoterephthalic acid and 0.94g sodium formate in 36.0 ml ethanol; the other steps remained the same.

2.3 Preparation of HKUST-1(NH_2-HKUST-1)/PEI mixed matrix membranes

Polyetherimide matrix solution (5.0 w.t. %) was obtained by dissolving pre-dried treated PEI particles (0.25 g) in dichloromethane (5.0 g) until the mixture became a clear uniform viscous solution. This concentration of the matrix solution was beneficial for the dispersion of the MOF crystals uniformly in the casting solution. Casting solution was prepared by dispersing different amounts of fillers (HKUST-1 and NH_2-HKUST-1 crystals after being vacuum-dried overnight) in the PEI matrix solution, via three rounds of magnetic stirring (10 min) and sonication (10 min) to ensure the uniformity of crystal particles. After thorough de-bubbling, the casting solutions were carefully poured onto a horizontally placed glass plate, and scraped by an automatic coating machine. The prepared mixed matrix membranes loading HKUST-1 and NH_2-HKUST-1 crystals cloud be taken from the glass plate after the solvent (CH_2Cl_2) was completely removed by drying at 25 °C, 60 °C, and 120 °C for 24h. The loading amount of HKUST-1 and NH_2-HKUST-1 crystals in the membranes was 10.0 w.t. % and 30 w.t. %, and these membranes were denoted as HKUST-1-10%/PEI, HKUST-1-30%/PEI, NH_2-HKUST-1-10%/PEI, and NH_2-HKUST-1-30%/PEI, respectively. The pristine PEI membrane was prepared without the addition of any HKUST-1 and NH_2-HKUST-1 crystals.

2.4 Characterization

X-ray diffraction (XRD, Bruker D8 Advance) was used to characterize the crystalline phase and structure of HKUST-1 and NH_2-HKUST-1 nanocrystals with a scanning rate of 2° min^{-1} in the 3-90° 2 *Theta* range, and the mixed matrix membranes with a scanning rate of 8° min^{-1} in the 3-75° 2 *Theta* range. Scanning electron microscope (SEM, JEOL-7900F) was applied to observe the crystal morphology and particle size of HKUST-1 and NH_2-HKUST-1 crystals and the top-view and cross-sectional surface features of mixed matrix membranes. Elementar (ELEMENTAR, UNICUBE) did the

element analysis (EA) under CHNS mode. Infrared spectrometer (Bruker Vertex 70V) recorded the fourier transform infrared (FT-IR) spectra of both MOFs crystals and MMMs with an average 64 scans in the 400-4000 cm^{-1} range. X-Ray photoelectron spectroscopy (XPS) was obtained by an ESCALAB 250Xi ThermoFischer spectrometer with an Al Kα source gun. N_2 sorption measurements were carried out on a Quantachrome, Autosorb IQ instrument to study the porous structure of HKUST-1 and NH_2-HKUST-1 crystals at -196 °C. H_2 and CO_2 adsorption capacities were also measured by a Quantachrome, Autosorb IQ instrument at 0 °C and 25 °C, and the measurement was taken at 0 °C for crystal sample. The degassing condition of the samples was 120 °C for 10 h. Thermogravimetric analyses (TG and DSC) were performed from 35 °C to 800 °C under nitrogen atmosphere with a 5 °C min^{-1} heating rate by using a NETZSCH (STA 449 F5) analyzer

2.5 Gas separation performance test of MMMs

The gas separation performance test was based on the Wicke-Kallenbach technique. Before testing, membranes were activated at 120 °C for 24h under vacuum. Then, all the mixed matrix membrane were place a stainless-steel module with an effective membrane area of 1.77 cm^2. Both the one-component gas (H_2, CO_2) permeability and mixed two-component gas permeability and separation (H_2/CO_2) would be characterized. The flow rate of feed gas was 100 ml min^{-1}, and the flow rate of sweeping gas (Ar) at the permeate side was 40 ml min^{-1} in order to avoid concentration polarization. For two-component mixed gas, the gas flow ratio was 1:1. A transmembrane pressure drop of 0.5 bar was maintained for all tests. The composition of the permeated gases was detected by a gas chromatography (Scion, 456-GC). Each membrane sample would be tested at least 3 times to get the average permeation data. The gas permeability of component *i* (P_i) in *Barrer* (1 *Barrer* =1 × 10^{-10} cm^3 (STP)·cm·$cm^{-2}s^{-1}$·$cmHg^{-1}$) of mixed matrix membranes was evaluated based on Equation (1):

$$P_i = \frac{10^{-10} l N_i}{A \Delta p_i} \qquad (1)$$

where N_i is the volume flow rate (cm^3(STP)·s^{-1}), l is the membrane's thickness (m), ΔP_i is the transmembrane pressure drop (cmHg), and A is the effective membrane's area (m^2).

The MMMs' selectivity ($\alpha_{i/j}$) was calculated according to Equation (2):

$$\alpha_{i/j} = \frac{X_i/X_j}{Y_i/Y_j} \qquad (2)$$

where X_i/X_j and Y_i/Y_j are the volumetric fractions of the permeate and feed gas, respectively.

2.6 Thermodynamic calculation of gas permeation behavior of MMMs

In this work, E_P, E_D and ΔH_S were used to describe the permeation behavior of gases in MMM, which are the activation energies of permeation and diffusion and enthalpy

of sorption[24, 25]. The relation between E_P, E_D and ΔH_S is presented by Equation (3):

$$E_P = E_D + \Delta H_S \qquad (3)$$

E_P was calculated according to the Arrhenius empirical Equation (4):

$$\ln P = \mathrm{a} - \frac{E_P}{RT} \qquad (4)$$

Where P is the gas permeability, T is the measurement temperature (K), and R is the ideal gas constant.

ΔH_S can be calculated using the Clausius-Clapperron Equation (5):

$$\ln p = \frac{\Delta H_S}{R}\frac{1}{T} + C \qquad (5)$$

Where p (MPa) is the testing pressure, T (K) is the measurement temperature, and R is the ideal gas constant.

3 Results and discussion

3.1 Structure analysis of NH_2-HKUST-1 and HKUST-1 samples

The X-Ray diffraction patterns of NH_2-HKUST-1 and HKUST-1 samples, together with a simulated XRD pattern of HKUST-are shown in Figure 1 a-c. The characteristic peaks for NH_2-HKUST-1 and HKUST-1 assigned to (111), (200), (220), (222), and (400) planes are present in the patterns and they are in good agreement with the simulated XRD, thus indicating the purity of the *in-situ* amino-modified sample. Assuming that the crystallinity of the HKUST-1 is 100%, the relative crystallinity of the NH_2-HKUST-1 is 88.52%. The average crystal size of HKUST-1 determined using Scheller's formula is 110 nm and of NH_2-HKUST-1 is 70 nm. The difference in crystal size was also confirmed by SEM (Figure S1). The changes in crystallinity and crystal size of NH_2-HKUST-1 are probably due to the introduction of hetero-structured amine based organic ligands (2-Aminoterephthalic acid). The deprotonation ability of 2-Aminoterephthalic acid ($pK_a \approx 3.95$) is stronger than that of trimesic acid ($pK_1=2.12$, $pK_2=4.10$, $pK_3=5.18$), causing 2-Aminoterephthalic acid to act as an capping agent thus inhibiting further growth of the crystals and leading to the reduction of the crystal size. The structures of HKUST-1 and NH_2-HKUST-1 samples have been refined and a slight increase of crystal cell parameter *a* from 26.32 to 26.33 Å after amination, due to the partial substitution of organic ligands in the crystal structure is observed for NH_2-HKUST-1 sample.

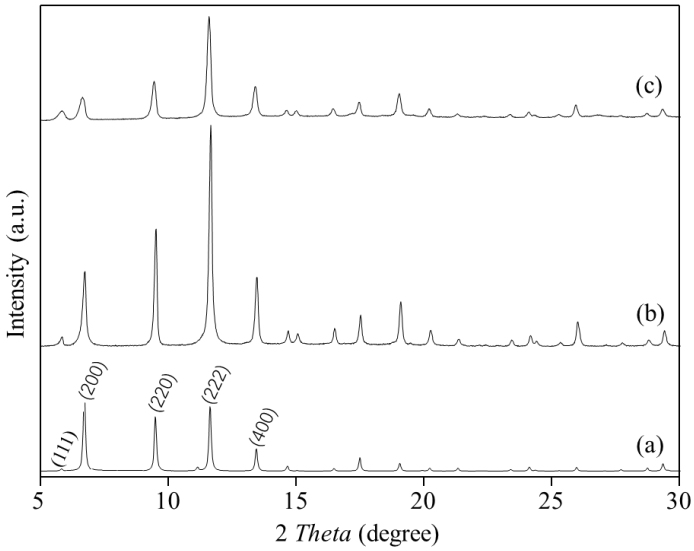

Figure 1 XRD patterns of (a) HKUST-1 (simulated), (b) HKUST-1 and (c) NH_2-HKUST-1 samples

The substitution ratio of the 2-aminoterephthalic acid in the NH_2-HKUST-1 was calculated based on the elemental analysis (Table S1). The ratio of m (2-aminoterephthalic acid): m (1,3,5-trihydroxybenzene) is calculated to be 1 : 5, which is lower than the feeding ratio 1 : 2 in the initial precursor mixture. Based on the XPS result (Figure S2), the ratio of m (2-aminoterephthalic acid): m (1,3,5-trihydroxybenzene) (1 : 1.3) of the outer surface of NH_2-HKUST-1 was found to be higher than that of the bulk crystals suggesting the role of amine ligand as an inhibitor. Thus we hypothesized that the amino-modified NH_2-HKUST-1 sample exhibits a "core-shell" structure as schematically presented in Figure 2. Due to the capping effect of the 2-aminoterephthalic acid entering the skeleton, the crystals stop growing, forming an outer surface with a higher amino ligand concentration.

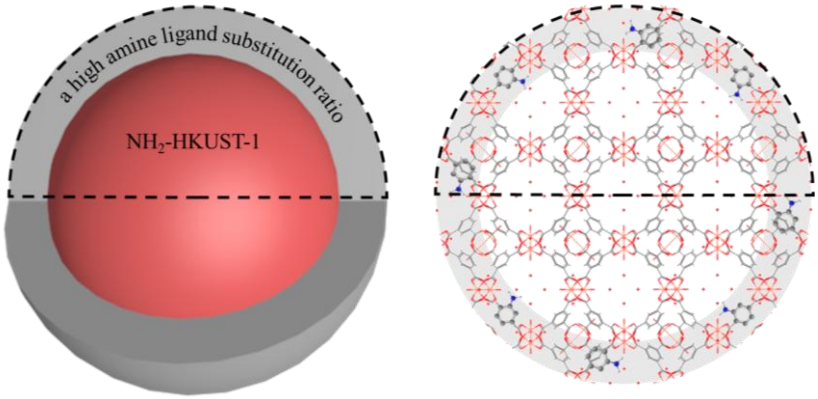

Figure 2 Schematic presentation of NH_2-HKUST-1 "core-shell" structure: the gray band is the outer surface of NH_2-HKUST-1 crystals with a higher amine ligand (2-aminoterephthalic acid) amount

The effect of amination on the crystals porous structure was studied by nitrogen adsorption (Figure 3). After amination, the HKUST-1 and NH_2-HKUST-1 samples show a reduction of the BET surface area from 792.5 m^2g^{-1} to 662.3 m^2g^{-1}, respectively. While, the external surface area increased, due to the smaller particle

size of NH_2-HKUST-1, the micropore volume decreased. The pore size remained the same in both samples, which is consistent with XRD results. However, the decrease of pore volume from 0.30 cm^3/g to 0.23 cm^3/g indicates the occupation of the pores by -NH_2 groups.

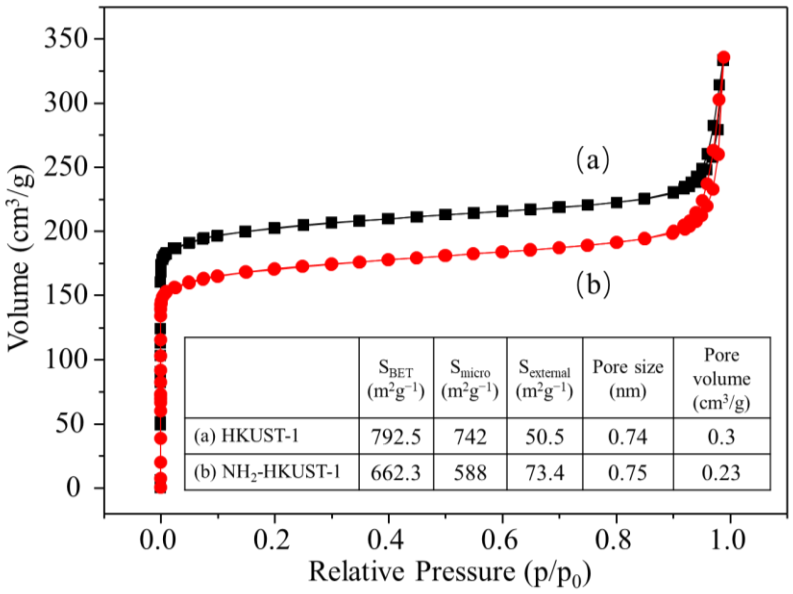

	S_{BET} (m^2g^{-1})	S_{micro} (m^2g^{-1})	$S_{external}$ (m^2g^{-1})	Pore size (nm)	Pore volume (cm^3/g)
(a) HKUST-1	792.5	742	50.5	0.74	0.3
(b) NH_2-HKUST-1	662.3	588	73.4	0.75	0.23

Figure 3 N_2 adsorption isotherms of (a) HKUST-1 and (b) NH_2-HKUST-1 recorded at --196 °C; ***Inset:*** **results deduced from the N_2 adsorption measurements.**

The adsorption results of HKUST-1 and NH_2-HKUST-1 samples further confirmed the occupation of the pore space by the -NH_2 groups. Additionally, the NH_2-HKUST-1 exhibits lower CO_2 adsorption capacity as shown in Figure S3 in contrast to previous reports on surface functionalized MOFs materials[26, 27]. This result can be explained with the reduced free pore volume of NH_2-HKUST-1 occupied by the amino groups. The decreased adsorption rate indicates that the amino groups do not act as active sites on NH_2-HKUST-1's surface.

The form of the 2-aminoterephthalic acid ligand in the NH_2-HKUST-1 structure under the action of the central metal Cu^{2+} was calculated using the pm6[28] method of Gaussian[29]. The binding energy of –NH_2 groups in the pores of the NH_2-HKUST-1 is -348.51 kJ/mol, while outside, at the surface of the crystals is -339.77 kJ/mol (Figure 4). This result indicates that amino groups are more likely to be confined in the channels of the NH_2-HKUST-1 which is consistent with the N_2 adsorption results presented above.

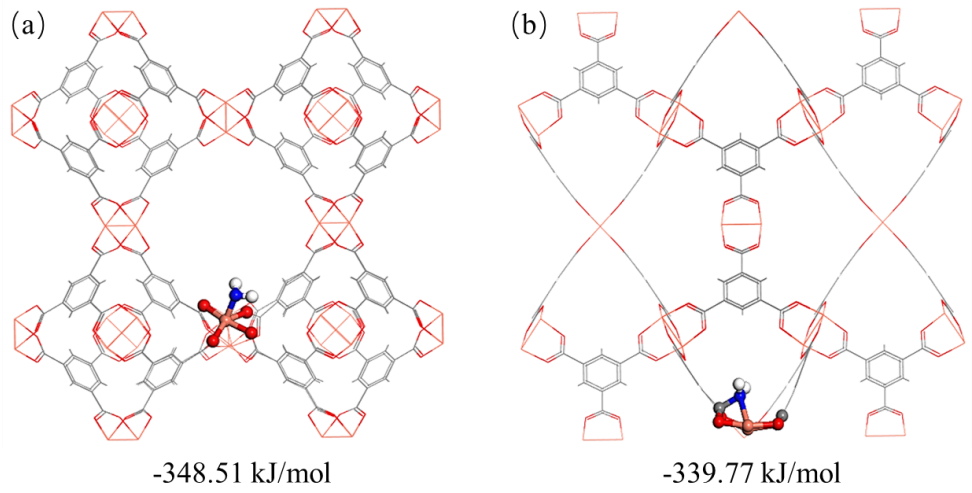

Figure 4 Binding energy of amino group in the NH_2-HKUST-1 sample: (a) inside the channels and (b) outside the crystals

In order to further prove that the amino ligand enters in the pores of the crystals, both samples HKUST-1 and NH_2-HKUST-1 were subjected to FT-IR charcatreization (Figure 5). The bands corresponding to the vibrations of C-O (1375 cm^{-1}), benzene ring (1564 cm^{-1}) and C=O (1644 cm^{-1}) are observed in both samples. Two new bands in the spectrum of NH_2-HKUST-1's at 3237 cm^{-1} and 3151 cm^{-1} appeared and they are attributed to the vibration of N-H[21, 30] (Figure 5b). Also the peak at 1687 cm^{-1} is related to -NH_2[15]. The bands at 1161 cm^{-1} and 1545 cm^{-1} are corresponding to the C-N bond[21]. The new bands proved the presence of amino groups in NH_2-HKUST-1 sample.

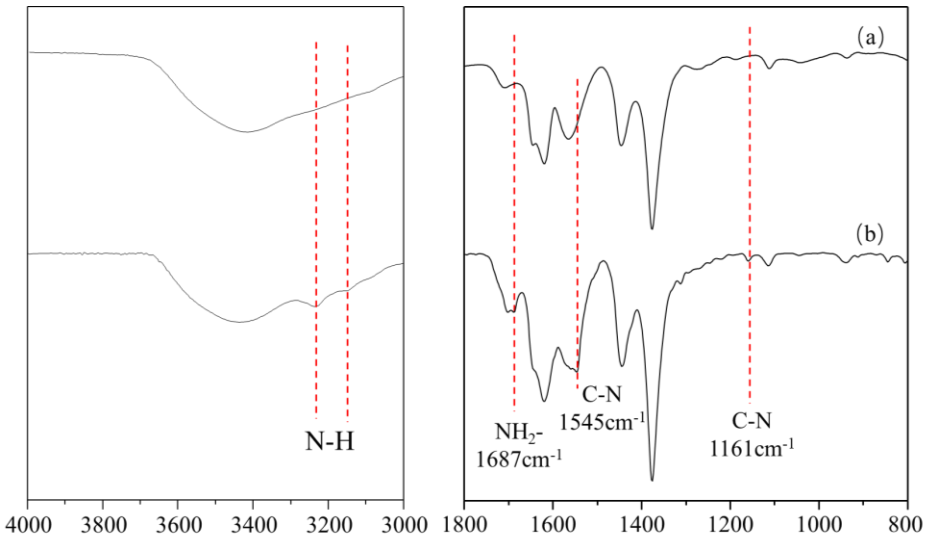

Figure 5 FT-IR spectra of (a) HKUST-1 and (b) NH_2-HKUST-1 crystals

The TG study of both HKUST-1 and NH_2-HKUST-1 reveals the structural change at 270 °C and a residual mass of around 40% suggesting that the amine ligand has little effect on the structure (Figure S4). Before the decomposition and combustion of the organic ligand (270 °C), the weight loss of MOF crystal is mainly due to dehydration process, including the first step related to the removal of physically absorbed water

and the second step related to the release of chemisorbed water[31, 32]. Two endothermic peaks between 100 °C and 270 °C could be observed from the DTG curves (Figure S4 inserted figure), which correspond to the two dehydration processes. In NH_2-HKUST-1, the first physical dehydration step ended at 187 °C, higher than that in HKUST-1 (164 °C), due to the stronger interaction formed by amino groups and water molecules. Additionally, the thermal degradation of NH_2-HKUST-1 started at a lower temperature, due to the -NH_2 groups which decomposed at lower temperature[33].

3.2 Structural analysis of membranes

In our previous work we demonstrated that loading of crystals in the membranes with less than 30% can avoid their agglomeration[18]. Therefore, in this work, we will focus on the MMMs with 10% and 30% filling amount. Seen from Figure S5, mixed matrix membranes with different amounts of fillers have XRD patterns belonging to PEI and MOF crystals, proving that HKUST-1 maintained its structure during the membrane preparation. The intensity of crystal peaks of MMMs with the same filler enhanced with the increase of loading amount. The signal intensity of HKUST-1 filled membranes are more obvious than that of NH_2-HKUST-1 filled membranes, which is consistent with crystals' XRD patterns (Figure 1).

As can be seen in SEM images (Figure S6), all the mixed matrix membranes are continuous and the HKUST-1 particles are evenly distributed. It is worth noting that when the filling amount reaches 30%, the cross-section morphology of HKUST-1-30%/PEI MMM exhibited more obvious polymer veins than that of NH_2-HKUST-1-30%/PEI, which was caused by plastic deformation[34]. This was related to the different interaction strength between the NH_2-HKUST-1 crystals and the PEI, which will be discussed below.

Compared with membranes with HKUST-1 (HKUST-1-10%/PEI and HKUST-1-30%/PEI), the NH_2-HKUST-1-10%/PEI and NH_2-HKUST-1-30%/PEI show an additional peak at 3237 cm^{-1} representative of N-H bond[21] (Figure S7). Previous works reported on amino-functional fillers forming hydrogen bonds with organic matrix, and the vibration of -NH_2 showed a significant blue shift[26, 35, 36]. While, no significant shift of this peak in the NH_2-HKUST-1-10%/PEI and NH_2-HKUST-1-30%/PEI membranes is observed, indicating that the chemical environment of N-H bond has not changed after loading in PEI matrix. It is suggested that the amino groups are mainly present in the pores rather than on the outer surface. The C=O band belonging to the PEI's 5-membered ring due to react with the Cu^{2+} unsaturated metal sites exhibits an obvious blue shift in all samples. In the HKUST-1-30%/PEI MMM (Figure S7 c), the C=O band shifts from 1777.3 cm^{-1} to 1779.8 cm^{-1}. However, in the NH_2-HKUST-1-30%/PEI (Figure S7 e), the band shifting is less only from 1777.3 cm^{-1} to 1778.3 cm^{-1}. The electron donor -NH_2 group leaded to an increase in the electron cloud density of the NH_2-HKUST-1 crystal, which might weakened the interaction between the PEI polymer and NH_2-HKUST-1

crystals in the membranes. In summary, the amination of HKUST-1 does not improve the interactions between the NH_2-HKUST-1 and the PEI as expected.

The XPS results also showed that the interaction between NH_2-HKUST-1 and PEI was not further enhanced. The XPS spectra for Cu $2p_{3/2}$ of the pure crystals and membranes are shown in Figure S8. The XPS spectra of HKUST-1 (Figure S8a) and NH_2-HKUST-1 (Figure S8b) contain a distinct peak at 934.97 eV and 934.95 eV, and a satellite peaks ranged from 948 eV to 937 eV[37, 38], respectively. The NH_2-HKUST-1(Cu) is similar to HKUST-1(Cu), suggesting that the -NH_2 groups do not coordinate with Cu^{2+} but may be protruding into the pores[39]. By comparing the spectra recorded on the membranes and pure HKUST-1, NH_2-HKUST-1 crystals, the signal intensity of Cu $2p_{3/2}$ decreased. In the HKUST-1-30%/PEI membrane, the peak shift is due to the effect of C=O on Cu^{2+} resulting in an increase of the electron cloud density of Cu^{2+}. While, the shift decreases for the NH_2-HKUST-1-30%/PEI membrane, confirming the weakened interactions.

The TG of the membranes shows a significant inflection point around 300 °C, which is consistent with the TG results of pure HKUST-1, NH_2-HKUST-1 materials, resulting from the collapse of their structure (Figure S9). DSC analysis before 300 °C reveals the glass transition temperature (*Tg*) of the PEI polymer. Glass transition temperature reflects the lowest temperature at which molecular segments in a polymer can move. As can be seen from Figure 6, the *Tg* rises after filling appropriate amount of HKUST-1 and NH_2-HKUST-1 particles. The HKUST-1-30%/PEI membrane with the strongest interactions between PEI matrix and HKUST-1 crystals, has the highest Tg of 213.6 °C, thus further explaining the higher effect of HKUST-1 than NH_2-HKUST-1 on the PEI.

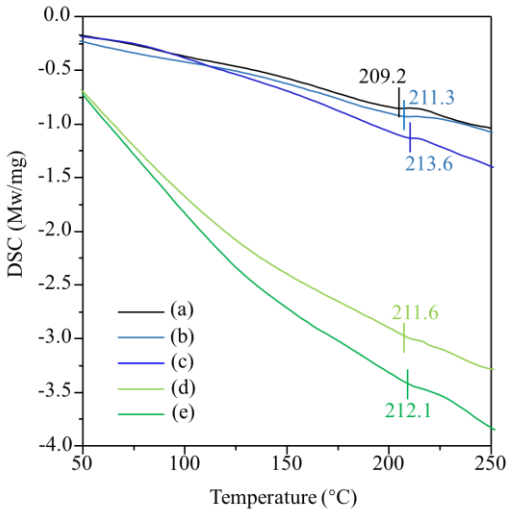

Figure 6 Differential scanning calorimetry (DSC) curves of (a) pure PEI membrane, (b) HKUST-1-10%/PEI, (c) HKUST-1-30%/PEI, (d) NH_2-HKUST-1-10%/PEI and (e) NH_2-HKUST-1-30%/PEI with the glass transition temperature (*Tg*)

3.3 Gas separation performance of membranes

The H_2 and CO_2 single gas permeability of the pure PEI membrane and the mixed

matrix membranes were measured at 25 °C. The permeability and ideal selectivity obtained for all membranes are depicted in Figure 7 and summarized in Table S2. Overall, the H_2 permeability and selectivity of the MMMs improved with the addition of both HKUST-1 and NH_2-HKUST-1 compared with the parent PEI membrane. With the increase of the loading amount of the same filler (HKUST-1 or NH_2-HKUST-1), the H_2 permeability increased. However, all MMMs exhibited reduced CO_2 permeability, suggesting that both HKUST-1 and NH_2-HKUST-1 fillers did not affect the CO_2 permeance. The different trends in permeability of H_2 and CO_2 stated that the effect of non-selective interface defects was low in MMMs. This is consistent with the results presented in Figure S7, where the interactions between the filler (HKUST-1 and NH_2-HKUST-1) and the PEI matrix were proved.

In order to further understand the effect of amino-modification of HKUST-1 on MMMs, the performance of NH_2-HKUST-1-30%/PEI and HKUST-1-30%/PEI was compared. NH_2-HKUST-1 sample has smaller crystal size than the HKUST-1 (Figure S1). Generally, the reduction in crystal size leads to enhanced interfacial forces between the filler and the matrix. While, according to the IR and TG analysis of MMMs, we found that the interfacial interactions were not enhanced in the NH_2-HKUST-1-30%/PEI membrane. Therefore, we assume that the effect of interfacial voids caused by size reduction has little effect on membrane's permeability. The lower permeability of NH_2-HKUST-1-30%/PEI membrane for both H_2 and CO_2 was mainly due to the pore blockage by -NH_2 groups. While, there was a little increase in ideal selectivity from 21.0 (HKUST-1-30%/PEI) to 21.9 (NH_2-HKUST-1-30%/PEI), since the diffusion of large CO_2 molecule was more easily limited by the narrowed diffusion channels. Thus, the amino groups located in the pores caused a loss of membranes' permeability; there membranes (NH_2-HKUST-1-10%/PEI and NH_2-HKUST-1-30%/PEI) were not subjected to optimization.

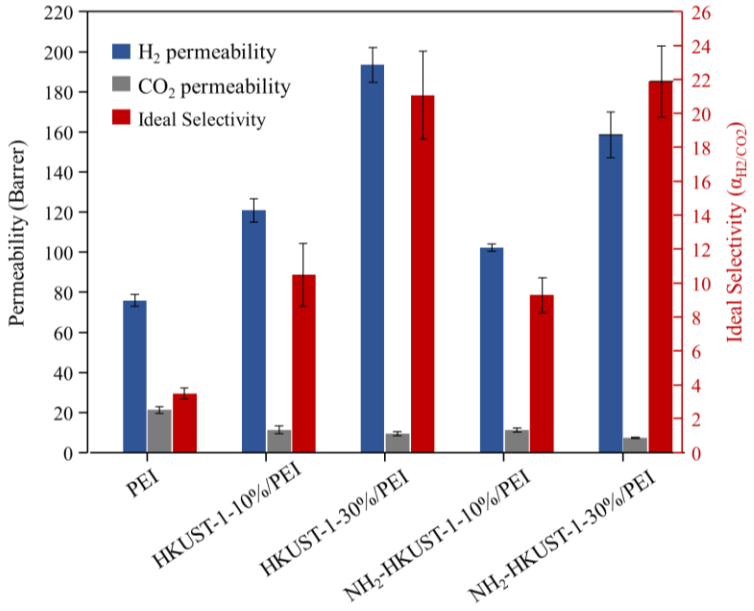

Figure 7 Single gas separation performance of pristine PEI membrane and mixed

matrix membranes HKUST-1/PEI and NH_2-HKUST-1 measured at 25 °C

The mixed gas separation performance of the MMMs has the similar trend as the single component gas separation testing (Figure 8 and Table S3). The NH_2-HKUST-1-30%/PEI membrane showed a decrease gas permeability for both H_2 and CO_2 with a slight improved selectivity. However, due to the competitive adsorption of H_2 and CO_2, the mixed gas separation performance (both permeability and selectivity) of this membrane was lower than that of the single component gas separation performance.

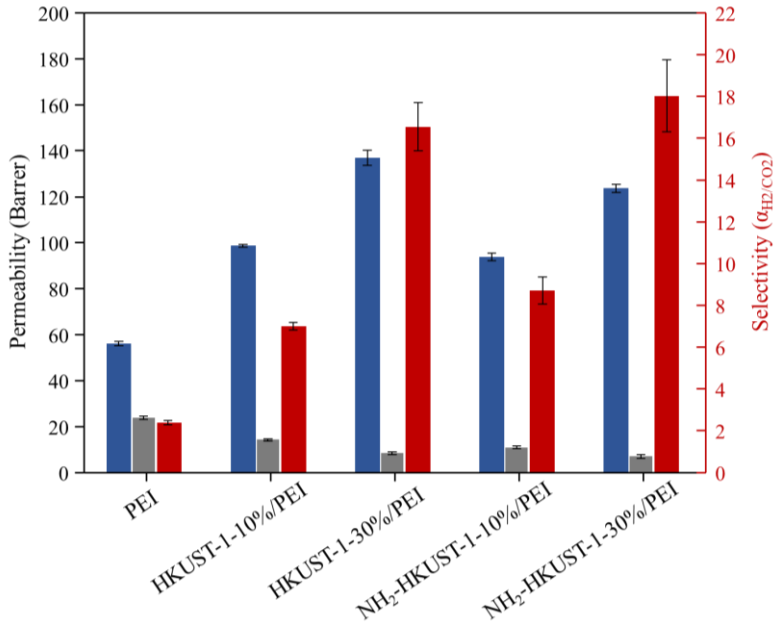

Figure 8 Mixed gas separation performance of pristine PEI membrane and mixed matrix membranes HKUST-1/PEI and NH_2-HKUST-1 measured at 25 °C

The Robeson upper boundary (2008) was used to evaluate the H_2/CO_2 separation performance of HKUST-1-30%/PEI and NH_2-HKUST-1-30%/PEI MMMs (Figure 9 and Table S5)[40]. First, we found that the H_2/CO_2 separation performances of PEI-based MMMs, filling small pore MOFs (such as ZIF-8, ZIF-90, ZIF-12), were close to the upper boundary. Compared with pure PEI membranes, the main contribution of filler materials was the improvement of H_2 permeability. After adding HKUST-1 or NH_2-HKUST-1, the H_2 permeability of HKUST-1-30%/PEI and NH_2-HKUST-1-30%/PEI MMMs was improved more significantly, and the selectivity also increased. As HKUST-1 does not have molecular sieving property for H_2/CO_2 separation, its highly permeable channels mainly contributed to the performance's optimization under the "adsorption-diffusion coupling control" mechanism. Nevertheless, the amino-functionalization exhibited a negative effect on the high permeability of MMMs due to the pore blockage. Second, there is a performance gap between our work and other high efficient MMMs, which is mainly related to the intrinsic separation performance of the matrix materials. Efficient matrices, such as polybenzimidazole (PBI), polyimides (PIs), and polymers of intrinsic microporosity (PIMs), generally exhibit high intrinsic gas permeability and selectivity. However, the price, synthesis process, processibility and mechanical strength of matrices should

also be considered. The PBI matrix is an expensive and difficult to process, the PIMs matrix shows poor mechanical properties. Compared with them, the PEIs showed high mechanical stability and economically viable for applications.

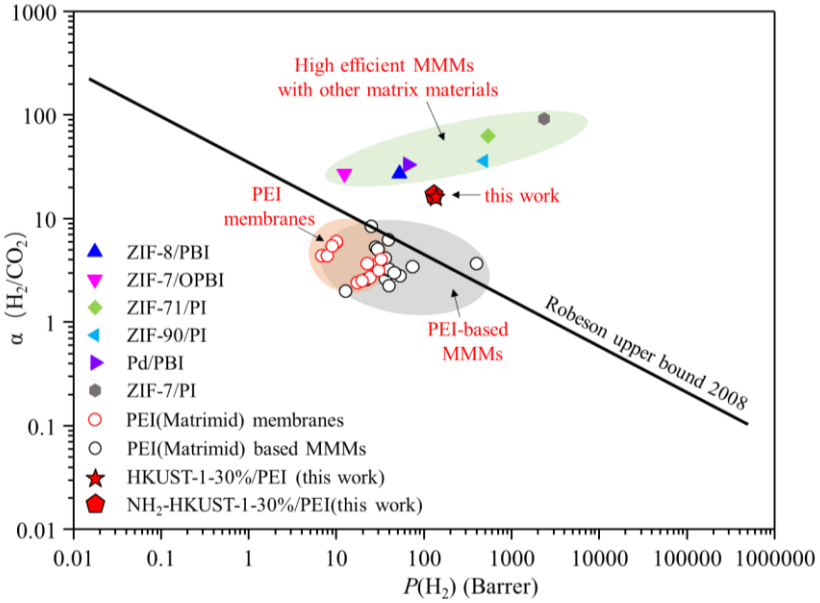

Figure 9 H_2/CO_2 separation performance of MMMs via Robeson upper bound (2008)[40]; details are shown in Table S5[41, 60]

As discussed in the introduction section, the main challenge for MMMs for H_2/CO_2 separation is the high adsorption and solubility of CO_2 in MMMs, which results in lower H_2/CO_2 selectivity compared to other gas pairs that requires high CO_2 permeability, such as CO_2/CH_4. This work provides new strategy to achieve H_2/CO_2 separation by utilizing HKUST-1 crystals with big pores. While, the amino-functionalization of the HKUST-1 crystals leading to pore blockage has a negative effect on the separation.

3.4 Gas separation mechanism

In our previous work, we reported the "adsorption-diffusion coupling control" separation mechanism under addition of large-pore HKUST-1 in the MMM for separation of small H_2 molecules from CO_2 molecules, thus suggesting the diffusion control H_2 permeation and adsorption prevention of CO_2 permeation[18]. Here, we studied the role of amino groups in the HKUST-1 crystals. According to the gas separation results, we found that the diffusion of gas molecules was blocked by the amino-functional groups of the NH_2-HKUST-1-30%/PEI mainly occupying the permeable channels, resulting in decreased permeability for both H_2 and CO_2. In addition, the small NH_2-HKUST-1 crystals used in this work did not show obvious enhancement of the interfacial voids. Thermodynamic study was used to elucidate the pore blockage and adsorption effect of $-NH_2$ groups (Table 1 and Figure S4). Firstly, the activation energy of permeation (E_P) of the small H_2 molecules is lower than that of the big CO_2 molecules, resulting in high H_2/CO_2 selectivity of the membranes. Secondly, the decreased $\Delta H_{S\ (H2\ and\ CO2)}$ of NH_2-HKUST-1-30%/PEI membrane

showed that the amino groups has little effect on the adsorption property of the MMMs, which may be due to the unexposed adsorption sites. The higher $E_{D(H2\ and\ CO2)}$ for NH_2-HKUST-1-30%/PEI than for HKUST-1-30%/PEI probably is resulted from the pore blockage. The $\Delta E_{D(CO2)}$ is bigger than the $\Delta E_{D(H2),}$ indicating that the pore blockage with $–NH_2$ groups had a greater effect on the CO_2 molecules. Thereby, the presence of amino groups in the HKUST-1's pores results in pore blockage, and eventually led to the deterioration of the membranes permeability.

Table 1 Thermodynamic calculations of mixed matrix membranes

Gas	Membrane	E_P (kJ/mol)	ΔH_S(kJ/mol)	E_D (kJ/mol)
H_2	HKUST-1-30%/PEI	5.3	-12.4	17.7
	NH_2-HKUST-1-30%/PEI	6.0	-11.9	17.9
CO_2	HKUST-1-30%/PEI	10.9	-24.8	35.7
	NH_2-HKUST-1-30%/PEI	15.8	-21.8	37.6

4 Conclusions

NH_2-HKUST-1 was synthesized successfully and thoroughly characterized in comparison to the parent HKUST-1 sample. FT-IR results confirmed the introduction of $–NH_2$ in the HKUST-1's sample. The crystallinity and spatial distribution of amino groups showed that the amino ligand (2-Aminoterephthalic acid) mainly is present on the outer surface of NH_2-HKUST-1 due to the end-capping effect, forming a "core-shell" crystal structure. While, the N_2 adsorption results and theoretical calculation suggested that the $-NH_2$ groups of the ligand tend to be constrained in the pores of NH_2-HKUST-1 crystals under the action of Cu^{2+} resulting in pore blockage. As a result, the mixed matrix membranes prepared (NH_2-HKUST-1/PEI) did not exhibit enhanced interfacial interactions. Furthermore, the pore blockage seriously affected the diffusion of the gas molecules, leading to decrease of the gas permeability of the NH_2-HKUST-1-30%/PEI membrane. Despite the little improvement in selectivity, the sacrifice of permeability makes the amino-modification not an appropriate optimization strategy for preparation of MMMs. This work demonstrated the negative effect of amino-modification/functionalization to the HKUST-1 materials on MMMs performance. Further the spatial distribution of amino groups in the HKUST-1 should be considered and optimize prior using for MMMs fabrication.

Declaration of Competing Interest

The authors declare that they have no known competing financial interests or personal relationships that could have appeared to influence the work reported in this paper.

Acknowledgements

This work was supported by National Key Research and Development Program of China of Ministry of Science and Technology (2022YFE0116000), National Natural

Science Foundation of China (No. 22175200, No. 21975285), the Fundamental Research Funds for the Central Universities (No. 21CX06024A), and Qingdao Postdoctoral Research Project (No. qdyy20210005), Fujian Province Science and Technology Program, Innovation Fund (2022C0021).

References

[1]L. Shao, B. T. Low, T. Chung, A. R. Greenberg, Polymeric Membranes for the Hydrogen Economy: Contemporary Approaches and Prospects for the Future, J. Membrane Sci., 327 (2009) 18-31. https://doi.org/10.1016/j.memsci.2008.11.019.

[2]D. Sholl, R. Lively, Seven Chemical Separations to Change the World, Nature, 532 (2016) 435-437. https://doi.org/10.1038/532435a.

[3]M. Galizia, W. S. Chi, Z. P. Smith, T. C. Merkel, R. W. Baker, B. D. Freeman, 50Th Anniversary Perspective : Polymers and Mixed Matrix Membranes for Gas and Vapor Separation: A Review and Prospective Opportunities, Macromolecules, 50 (2017) 7809-7843. https://doi.org/10.1021/acs.macromol.7b01718.

[4]M. Ahmadi, S. Janakiram, Z. Dai, L. Ansaloni, L. Deng, Performance of Mixed Matrix Membranes Containing Porous Two-Dimensional (2D) and Three-Dimensional (3D) Fillers for CO_2 Separation: A Review, Membranes, 8 (2018) 1-50. https://doi.org/10.3390/membranes8030050.

[5]A. R. Kamble, C. M. Patel, Z. V. P. Murthy, A Review On the Recent Advances in Mixed Matrix Membranes for Gas Separation Processes, Renew. Sust. Energ. Rev., 145 (2021) 111062. https://doi.org/10.1016/j.rser.2021.111062.

[6]Q. Qian, P. A. Asinger, M. J. Lee, G. Han, K. Mizrahi Rodriguez, S. Lin, F. M. Benedetti, A. X. Wu, W. S. Chi, Z. P. Smith, MOF-Based Membranes for Gas Separations, Chem. Rev., 120 (2020) 8161-8266. https://doi.org/10.1021/acs.chemrev.0c00119.

[7]W. K. Setiawan, K. Chiang, Silica Applied as Mixed Matrix Membrane Inorganic Filler for Gas Separation: A Review, Sustain. Environ. Res., 29 (2019) 29-32. https://doi.org/10.1186/s42834-019-0028-1.

[8]D. Bastani, N. Esmaeili, M. Asadollahi, Polymeric Mixed Matrix Membranes Containing Zeolites as a Filler for Gas Separation Applications: A Review, J. Ind. Eng. Chem., 19 (2013) 375-393. https://doi.org/10.1016/j.jiec.2012.09.019.

[9]S. H. Goh, H. S. Lau, W. F. Yong, Metal–Organic Frameworks (MOFs)- Based Mixed Matrix Membranes (MMMs) for Gas Separation: A Review On Advanced Materials in Harsh Environmental Applications, Small, 18 (2022) 2107536. https://doi.org/10.1002/smll.202107536.

[10]Y. Cheng, S. J. Datta, S. Zhou, J. Jia, O. Shekhah, M. Eddaoudi, Advances in Metal-Organic Framework-Based Membranes, Chem. Soc. Rev., 51 (2022) 8300-8350. https://doi.org/10.1039/d2cs00031h.

[11]M. Kalaj, K. C. Bentz, S. Ayala, J. M. Palomba, K. S. Barcus, Y. Katayama, S. M. Cohen, MOF-Polymer Hybrid Materials: From Simple Composites to Tailored Architectures, Chem. Rev., 120 (2020) 8267-8302. https://doi.org/10.1021/acs.chemrev.9b00575.

[12]M. W. Anjum, F. Vermoortele, A. L. Khan, B. Bueken, D. E. De Vos, I. F. J. Vankelecom, Modulated UiO-66-Based Mixed-Matrix Membranes for CO_2 Separation,

ACS Appl. Mater. Inter., 7 (2015) 25193-25201. https://doi.org/10.1021/acsami.5b08964.
[13]H. Molavi, A. Shojaei, S. A. Mousavi, Improving Mixed-Matrix Membrane Performancevia Pmma Grafting From Functionalized NH_2–UiO-66, J. Mater. Chem. A, 6 (2018) 2775-2791. https://doi.org/10.1039/C7TA10480D.
[14]S. Meshkat, S. Kaliaguine, D. Rodrigue, Mixed Matrix Membranes Based On Amine and Non-Amine MiL-53(Al) in Pebax® MH-1657 for CO_2 Separation, Sep. Purif. Technol., 200 (2018) 177-190. https://doi.org/10.1016/j.seppur.2018.02.038.
[15]N. Tien-Binh, H. Vinh-Thang, X. Y. Chen, D. Rodrigue, S. Kaliaguine, Polymer Functionalization to Enhance Interface Quality of Mixed Matrix Membranes for High CO_2/CH_4 Gas Separation, J. Mater. Chem. A, 3 (2015) 1522-15213. https://doi.org/10.1039/c5ta01597a.
[16]Y. Pu, Z. Yang, V. Wee, Z. Wu, Z. Jiang, D. Zhao, Amino-Functionalized NUS-8 Nanosheets as Fillers in PIM-1 Mixed Matrix Membranes for CO_2 Separations, J. Membrane Sci., 641 (2022) 119912. https://doi.org/10.1016/j.memsci.2021.119912.
[17]F. N. Al-Rowaili, M. Khaled, A. Jamal, U. Zahid, Mixed Matrix Membranes for H_2/CO_2 Gas Separation-A Critical Review, Fuel, 333 (2023) 126285. https://doi.org/10.1016/j.fuel.2022.126285.
[18]Y. Wang, G. Yang, H. Guo, X. Meng, G. Kong, Z. Kang, R. Guillet-Nicolas, S. Mintova, Preparation of HKUST-1/PEI Mixed-Matrix Membranes: Adsorption-Diffusion Coupling Control of Small Gas Molecules, J. Membrane Sci., 643 (2022) 120070. https://doi.org/10.1016/j.memsci.2021.120070.
[19]F. Hamidavi, A. Kargari, A. Eliassi, Sorption and Permeation Study of Polyetherimide/Hydrophobic Silica Nanocomposite Membrane for Effective Syngas ($H_2/CO/CO_2$) Separation, Sep. Purif. Technol., 279 (2021) 119774. https://doi.org/10.1016/j.seppur.2021.119774.
[20]J. Hu, H. Cai, H. Ren, Y. Wei, Z. Xu, H. Liu, Y. Hu, Mixed-Matrix Membrane Hollow Fibers of $Cu_3(BTC)_2$ MOF and Polyimide for Gas Separation and Adsorption, Ind. Eng. Chem. Res., 49 (2010) 12605-12612. https://doi.org/10.1021/ie1014958.
[21]B. Ge, Y. Xu, H. Zhao, H. Sun, Y. Guo, W. Wang, High Performance Gas Separation Mixed Matrix Membrane Fabricated by Incorporation of Functionalized Submicrometer-Sized Metal-Organic Framework, Materials, 11 (2018) 1421. https://doi.org/10.3390/ma11081421.
[22]K. Pirzadeh, K. Esfandiari, A. A. Ghoreyshi, M. Rahimnejad, CO_2 and N_2 Adsorption and Separation Using Aminated UiO-66 and $Cu_3(BTC)_2$: A Comparative Study, Korean J. Chem. Eng., 37 (2020) 513-524. https://doi.org/10.1007/s11814-019-0433-5.
[23]Y. Wang, H. Ge, Y. Wu, G. Ye, H. Chen, X. Hu, Construction of an Electrochemical Sensor Based On Amino-Functionalized Metal-Organic Frameworks for Differential Pulse Anodic Stripping Voltammetric Determination of Lead, Talanta, 129 (2014) 100-105. https://doi.org/10.1016/j.talanta.2014.05.014.
[24]K. A. Stevens, J. D. Moon, H. Borjigin, R. Liu, R. M. Joseph, J. S. Riffle, B. D. Freeman, Influence of Temperature On Gas Transport Properties of Tetraaminodiphenylsulfone (TADPS) Based Polybenzimidazoles, J. Membrane Sci., 593 (2020) 117427. https://doi.org/10.1016/j.memsci.2019.117427.
[25]A. Fuoco, B. Satilmis, T. Uyar, M. Monteleone, E. Esposito, C. Muzzi, E. Tocci, M.

Longo, M. P. De Santo, M. Lanč, K. Friess, O. Vopička, P. Izák, J. C. Jansen, Comparison of Pure and Mixed Gas Permeation of the Highly Fluorinated Polymer of Intrinsic Microporosity PIM-2 Under Dry and Humid Conditions: Experiment and Modelling, J. Membrane Sci., 594 (2020) 117460. https://doi.org/10.1016/j.memsci.2019.117460.

[26]O. G. Nik, X. Y. Chen, S. Kaliaguine, Functionalized Metal Organic Framework-Polyimide Mixed Matrix Membranes for CO_2/CH_4 Separation, J. Membrane Sci., 413-414 (2012) 48-61. https://doi.org/10.1016/j.memsci.2012.04.003.

[27]H. Molavi, A. Shojaei, Mixed-Matrix Composite Membranes Based On UiO-66-Derived MOFs for CO_2 Separation, ACS Appl. Mater. Inter., 11 (2019) 9448-9461. https://doi.org/10.1021/acsami.8b20869.

[28]J. J. P. Stewart, Optimization of Parameters for Semiempirical Methods V: Modification of NDDO Approximations and Application to 70 Elements, J. Mol. Model., 13 (2007) 1173-1213. https://doi.org/10.1007/s00894-007-0233-4.

[29]M. Jfg, W. Trucks, H. B. Schlegel, G. E. Scuseria, M. A. Robb, J. R. Cheeseman, G. Scalmani, V. Barone, B. Mennucci, G. A. Petersson, Gaussian 09, Revision a. 1; Gaussian (2009).

[30]B. C. E. Silva, K. Irikura, R. C. G. Frem, M. V. B. Zanoni, Effect of Cu(BDC-NH_2) Mof Deposited On Cu/Cu_2O Electrode and its Better Performance in Photoelectrocatalytic Reduction of CO_2, J. Electroanal. Chem., 880 (2021) 114856. https://doi.org/10.1016/j.jelechem.2020.114856.

[31]F. Israr, D. K. Kim, Y. Kim, S. J. Oh, K. C. Ng, W. Chun, Synthesis of Porous Cu- BTC with Ultrasonic Treatment: Effects of Ultrasonic Power and Solvent Condition, Ultrason. Sonochem., 29 (2016) 186-193. https://doi.org/10.1016/j.ultsonch.2015.08.023.

[32]A. Domán, J. Madarász, K. László, In Situ Evolved Gas Analysis Assisted Thermogravimetric (Tg-FTIR and Tg/DTA–MS) Studies On Non-Activated Copper Benzene-1,3,5-Tricarboxylate, Thermochim. Acta, 647 (2017) 62-69. https://doi.org/10.1016/j.tca.2016.11.013.

[33]R. Abedini, M. Omidkhah, F. Dorosti, Highly Permeable Poly(4-Methyl-1-Pentyne)/NH_2-MiL53(Al) Mixed Matrix Membrane for CO_2/CH_4 Separation, RSC Adv. (2014) 36522-36537. https://doi.org/10.1039/C4RA07030E.

[34]E. V. Perez, K. J. Balkus, J. P. Ferraris, I. H. Musselman, Metal-Organic Polyhedra 18 Mixed-Matrix Membranes for Gas Separation, J. Membrane Sci., 463 (2014) 82-93. https://doi.org/10.1016/j.memsci.2014.03.045.

[35]Q. Xin, J. Ouyang, T. Liu, Z. Li, Z. Li, Y. Liu, S. Wang, H. Wu, Z. Jiang, X. Cao, Enhanced Interfacial Interaction and CO_2 Separation Performance of Mixed Matrix Membrane by Incorporating Polyethylenimine-Decorated Metal–Organic Frameworks, ACS Appl. Mater. Inter., 7 (2015) 1065-1077. https://doi.org/10.1021/am504742q.

[36]B. Zornoza, A. Martinez-Joaristi, P. Serra-Crespo, C. Tellez, J. Coronas, J. Gascon, F. Kapteijn, Functionalized Flexible MOFs as Fillers in Mixed Matrix Membranes for Highly Selective Separation of CO_2 From CH_4 at Elevated Pressures, Chem. Commun., 47 (2011) 9522-9524. https://doi.org/10.1039/c1cc13431k.

[37]A. S. Duke, E. A. Dolgopolova, R. P. Galhenage, S. C. Ammal, A. Heyden, M. D. Smith, D. A. Chen, N. B. Shustova, Active Sites in Copper-Based Metal–Organic Frameworks:

Understanding Substrate Dynamics, Redox Processes, and Valence-Band Structure, J. Phys Chem. C, 119 (2015) 27457-27466. https://doi.org/10.1021/acs.jpcc.5b08053.
[38]Y. Wu, H. Zhang, Y. Yan, J. Peng, High Efficient HKUST-1 Membrane Over Paper-Like Steel Fibers for Direct Catalytic Wet Peroxide Oxidation of Phenol, Mater. Chem. Phys., 252 (2020) 123119. https://doi.org/10.1016/j.matchemphys.2020.123119.
[39]H. Wang, X. Yuan, Y. Wu, G. Zeng, X. Chen, L. Leng, Z. Wu, L. Jiang, H. Li, Facile Synthesis of Amino-Functionalized Titanium Metal-Organic Frameworks and their Superior Visible-Light Photocatalytic Activity for Cr(Vi) Reduction, J. Hazard. Mater., 286 (2015) 187-194. https://doi.org/10.1016/j.jhazmat.2014.11.039.
[40]L. M. Robeson, The Upper Bound Revisited, J. Membrane Sci., 320 (2008) 390-400. https://doi.org/10.1016/j.memsci.2008.04.030.
[41]G. Li, Z. Si, S. Yang, Y. Zhuang, S. Pang, Y. Cui, J. Baeyens, P. Qin, A Defects-Free ZIF-90/6FDA-Durene Membrane Based On the Hydrogen Bonding/Covalent Bonding Interaction for Gas Separation, J. Membrane Sci., 661 (2022) 120910. https://doi.org/10.1016/j.memsci.2022.120910.
[42]X. Jiang, S. He, G. Han, J. Long, S. Li, C. H. Lau, S. Zhang, L. Shao, Aqueous One-Step Modulation for Synthesizing Monodispersed ZIF-8 Nanocrystals for Mixed-Matrix Membrane, ACS Appl. Mater. Inter., 13 (2021) 11296-11305. https://doi.org/10.1021/acsami.0c22910.
[43]M. Usman, M. Y. Khan, T. Anjum, A. L. Khan, B. Hoque, A. Helal, A. S. Hakeem, B. A. Al-Maythalony, Controlled Covalent Functionalization of ZIF-90 for Selective CO_2 Capture & Separation, Membranes, 12 (2022) 1055. https://doi.org/10.3390/membranes12111055.
[44]M. Boroglu, I. Boz, B. Kaya, Effect of New Metal-Organic Framework (Zeolitic Imidazolate Framework [ZIF-12]) in Mixed Matrix Membranes On Structure, Morphology, and Gas Separation Properties, J. Polym. Eng., 41 (2021) 259-270. https://doi.org/10.1515/polyeng-2020-0288.
[45]M. Safak Boroglu, M. Ugur, I. Boz, Enhanced Gas Transport Properties of Mixed Matrix Membranes Consisting of Matrimid and RHO Type ZIF-12 Particles, Chem. Eng. Res. Des., 123 (2017) 201-213. https://doi.org/10.1016/j.cherd.2017.05.010.
[46]S. Japip, K. Liao, Y. Xiao, T. Chung, Enhancement of Molecular-Sieving Properties by Constructing Surface Nano-Metric Layer Via Vapor Cross-Linking, J. Membrane Sci., 497 (2016) 248-258. https://doi.org/10.1016/j.memsci.2015.09.045.
[47]L. Hu, V. T. Bui, S. Pal, W. Guo, A. Subramanian, K. Kisslinger, S. Fan, C. Y. Nam, Y. Ding, H. Lin, In Situ Growth of Crystalline and Polymer- Incorporated Amorphous ZIFs in Polybenzimidazole Achieving Hierarchical Nanostructures for Carbon Capture, Small, 18 (2022) 2201982. https://doi.org/10.1002/smll.202201982.
[48]D. Carter, F. H. Tezel, B. Kruczek, H. Kalipcilar, Investigation and Comparison of Mixed Matrix Membranes Composed of Polyimide Matrimid with ZIF-8, Silicalite, and SAPO-34, J. Membrane Sci., 544 (2017) 35-46. https://doi.org/10.1016/j.memsci.2017.08.068.
[49]L. Diestel, N. Wang, A. Schulz, F. Steinbach, J. Caro, Matrimid-Based Mixed Matrix Membranes: Interpretation and Correlation of Experimental Findings for Zeolitic Imidazolate Frameworks as Fillers in H_2/CO_2 Separation, Ind. Eng. Chem. Res., 54 (2015) 1103-1112. https://doi.org/10.1021/ie504096j.

[50]S. Yang, Y. Wang, P. Lu, H. Jin, F. Pan, Z. Shi, X. Jiang, C. Chen, Z. Jiang, Y. Li, Metal–Organic Frameworks Corset with a Thermosetting Polymer for Improved Molecular-Sieving Property of Mixed-Matrix Membranes, ACS Appl. Mater. Inter., 12 (2020) 55308-55315. https://doi.org/10.1021/acsami.0c17426.
[51]R. Martinez-Tirado, N. Yuriychuk, M. Iglesias, M. López-González, E. M. Maya, Mixed Matrix Membranes Containing a Biphenyl-Based Knitting Aryl Polymer and Gas Separation Performance, Membranes, 11 (2021) 914. https://doi.org/10.3390/membranes11120914.
[52]M. Arjmandi, M. Pakizeh, Mixed Matrix Membranes Incorporated with Cubic-MOF-5 for Improved Polyetherimide Gas Separation Membranes: Theory and Experiment, J. Ind. Eng. Chem., 20 (2014) 3857-3868. https://doi.org/10.1016/j.jiec.2013.12.091.
[53]S. Zid, P. Alcouffe, M. Zinet, E. Espuche, Mixed-Matrix Membranes Based On Polyetherimide, Metal–Organic Framework and Ionic Liquid: Influence of the Composition and Morphology On Gas Transport Properties, Polymers, 14 (2022) 3489. https://doi.org/10.3390/polym14173489.
[54]Y. Zhang, K. J. Balkus, I. H. Musselman, J. P. Ferraris, Mixed-Matrix Membranes Composed of Matrimid® and Mesoporous ZSM-5 Nanoparticles, J. Membrane Sci., 325 (2008) 28-39. https://doi.org/10.1016/j.memsci.2008.04.063.
[55]E. V. Perez, K. J. Balkus, J. P. Ferraris, I. H. Musselman, Mixed-Matrix Membranes Containing MOF-5 for Gas Separations, J. Membrane Sci., 328 (2009) 165-173. https://doi.org/10.1016/j.memsci.2008.12.006.
[56]X. Ma, X. Wu, J. Caro, A. Huang, Polymer Composite Membrane with Penetrating ZIF- 7 Sheets Displays High Hydrogen Permselectivity, Angew. Chem. Int. Edit., 131 (2019) 16302-16306. https://doi.org/10.1002/ange.201911226.
[57]L. Zhu, D. Yin, Y. Qin, S. Konda, S. Zhang, A. Zhu, S. Liu, T. Xu, M. T. Swihart, H. Lin, Sorption- Enhanced Mixed Matrix Membranes with Facilitated Hydrogen Transport for Hydrogen Purification and CO_2 Capture, Adv. Funct. Mater., 29 (2019) 1904357. https://doi.org/10.1002/adfm.201904357.
[58]A. I. Romero, M. L. Parentis, A. C. Habert, E. E. Gonzo, Synthesis of Polyetherimide/Silica Hybrid Membranes by the Sol–Gel Process: Influence of the Reaction Conditions On the Membrane Properties, J. Mater. Sci., 46 (2011) 4701-4709. https://doi.org/10.1007/s10853-011-5380-4.
[59]M. Arjmandi, M. Pakizeh, O. Pirouzram, The Role of Tetragonal-Metal-Organic Framework-5 Loadings with Extra ZnO Molecule On the Gas Separation Performance of Mixed Matrix Membrane, Korean J. Chem. Eng., 32 (2015) 1178-1187. https://doi.org/10.1007/s11814-014-0315-9.
[60]Q. Song, S. K. Nataraj, M. V. Roussenova, J. C. Tan, D. J. Hughes, W. Li, P. Bourgoin, M. A. Alam, A. K. Cheetham, S. A. Al-Muhtaseb, E. Sivaniah, Zeolitic Imidazolate Framework (ZIF-8) Based Polymer Nanocomposite Membranes for Gas Separation, Energ. Environ. Sci., 5 (2012) 8359-8369. https://doi.org/10.1039/c2ee21996d.